Robust and optimal design of fixed structure controllers in collocated motion systems

Martin Goubej
NTIS research centre
University of West Bohemia
Pilsen, Czechia
mgoubej@ntis.zcu.cz

Jakub Tvrz
Department of Cybernetics
University of West Bohemia
Pilsen, Czechia
tvrzjak@students.zcu.cz

Břetislav Kubeš
Department of Cybernetics
University of West Bohemia
Pilsen, Czechia
bkubes@students.zcu.cz

***Abstract*—The paper deals with a methodology for the derivation of PI(D) type fixed structure controllers commonly embedded in motion control loops. A collocated control design problem is formulated, considering two different plant outputs. The goal is to tune the controller parameters to achieve both robustness in stability with respect to a feedback variable and optimal performance with respect to a second penalised output. The proposed method is validated by means of a lift control benchmark problem.**

***Index Terms*—optimal control, robust control, motion control systems, collocated control, velocity control, electrical drives, PID controllers, lift control**

I. Introduction

Modern mechatronic systems rely heavily upon properly designed and tuned motion control loops [1]. Practising engineers and technicians face the challenging task of setting up the parameters of motion controllers. The dynamics of the controlled plant is unique for each machine, requiring the control tuning to match the specifics of the particular system. The tuning process is commonly done manually, requiring a tedious trial-and-error procedure. The results are often suboptimal and depend on the skills of the persons involved.

The importance of proper tuning is pronounced with constantly increasing demands on the performance of industrial manufacturing systems that translate to the control layer in the form of strict requirements on achievable bandwidth and tracking precision in the case of motion systems [2]. Stringent performance requirements may introduce problems with mechanical vibrations once the target bandwidth overlaps with the resonance modes of the controlled plant. Unwanted transient and residual oscillations complicate the process of control system tuning. While automatic tuning methods were widely developed and successfully employed in practice in the field of process control [3], there is still a lack of suitable methods for mechatronic systems. Therefore, the development of systematic methods providing any support with the commissioning process is highly relevant for industrial practice.

This paper extends former results presented in [4]–[7], tailoring a generic algorithm of so-called H_∞ regions to a specific case of a collocated control setup, which is often encountered in motion systems. Section 2 formalizes the collocated control problem. Section 3 revises the previous results. Section 4 presents a novel framework allowing us to achieve both robustness and optimality in the resulting closed-loop system. Section 5 deals with the benchmark problem of designing a lift velocity control loop.

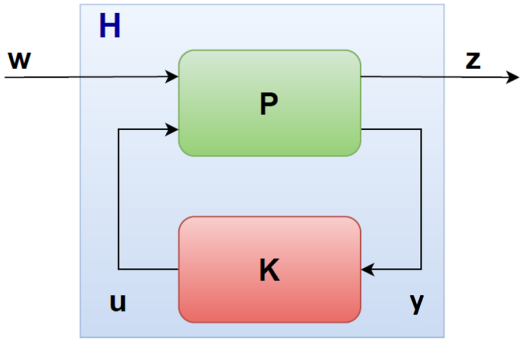

Fig. 1: Generic robust/optimal control setup

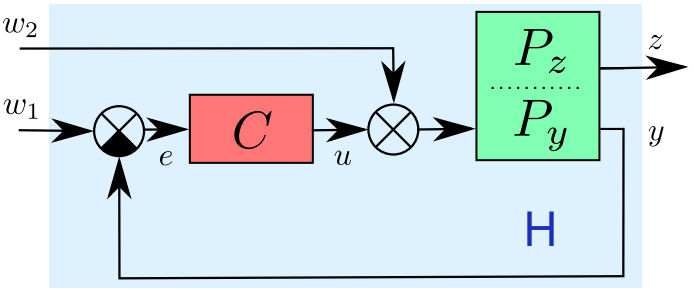

Fig. 2: Collocated control problem in a mechatronic system

II. Problem formulation - collocated control setup

We start with the generic setup shown in Fig. 1 that is commonly used in modern control theory methods to formulate optimal or robust feedback design problems. The goal is to derive a controller K that internally stabilizes the generalised plant P by forming a feedback loop via the measured outputs

y and manipulated variables u. Additionally, a performance measure quantifying a "gain" of the closed-loop system H is defined, often by means of H_2 or H_∞ system norms. An optimal K minimising the influence of the generalised disturbances w to the performance variables z in the sense of the chosen performance metric is then derived [8].

We assume a particular case of this generic setup shown in Fig. 2. This structure, often designated as a "collocated control setup", is very common in the field of mechatronics and motion control systems. The *collocated* term refers to the fact that the actuator-sensor pair is installed physically at the same location of the controlled plant. The measured output y used to close the velocity or position feedback loop is typically provided by an optical encoder attached directly to the rotor shaft of an electrical motor. On the other hand, the goal is to control another physical variable z; usually the position or velocity of some reference point at the load-side moving part, e.g. a robot end-effector or a CNC machine tool spindle. In the case of an ideally rigid load, the working mechanism and the attached actuator perform completely synchronous motions. In this case, the outputs coincide with each other (apart from potential scaling due to kinematic transform), and the control topology reduces to a standard single-input-single-output (SISO) feedback loop. However, the occurrence of mechanical flexibility in the driven load introduces additional degrees of freedom. More complex oscillatory behaviour with unwanted transient and residual oscillations often occurs due to plant bending modes. The fact that $y \neq z$ makes the feedback control design much more difficult. Excellent performance with respect to feedback variable y does not automatically guarantee a well-behaved response of the variable of true interest z.

Standard solutions of the generic optimal control problem generally lead to high-order controllers of order equal to the order of the generalised plant P, i.e. the order of the controlled plant plus additional dynamics of frequency-dependent weighting filters used to formulate user design requirements [9]. High-order controllers are difficult to implement in practice due to limitations of the target HW/SW platform or inherent sensitivity to finite precision floating-point calculations in digital processors. This is especially true for industrial motion control systems with limited CPU resources and control structure typically fixed to a low-order PI(D) compensator (plus optional feedback/reference/control action filters). Therefore, a direct derivation of a fixed structure low-order controller is generally more appropriate for such applications.

III. Previous results - H_∞ regions method

We now briefly revise results achieved at our workplace and presented in [4] that allow a systematic derivation of simple controllers with two or three parameters for the simpler 1DoF case ($y = z$) using so-called H_∞ regions method. This forms a baseline of the optimisation procedure we propose next for the collocated setup.

The controlled plant model is assumed in the form of LTI transfer function $P(s)$ without the poles on the imaginary axis. We consider a standard PI controller commonly used in industrial drive systems in the form of

$$C(s, \boldsymbol{k}) = k_p + \frac{k_i}{s}, \tag{1}$$

where $\boldsymbol{k} \triangleq [k_p, k_i]$ denotes the controller gains vector.

An arbitrary number of design constraints can be formulated in the frequency domain in the form of

$$||H(s, \boldsymbol{k})||_\infty < \gamma, \tag{2}$$

where H corresponds to an arbitrary closed-loop transfer function, commonly chosen as frequency weighted function

$$H(s, \boldsymbol{k}) \triangleq W(s) S_*(s), \tag{3}$$

where $S_*(s)$ denotes one of the closed-loop sensitivity functions (sensitivity, complementary-, input- and controller-sensitivity and $W(s)$ introduces arbitrary user-defined frequency-dependent scaling.

The goal is to find a controller $C(s, \boldsymbol{k})$ which together for the given $H(s)$ fulfills the following three conditions

1) $C(s, \boldsymbol{k})$ internally stabilizes the closed-loop
2) $H(s, \boldsymbol{k})$ used in the design criterion is stable
3) The H-infinity condition $||H(s, \boldsymbol{k})||_\infty < \gamma$ holds

Such a controller is called the H_∞ controller. Typically, a whole set $\mathcal{K}$ of the admissible controllers fulfilling the above-mentioned conditions exists and can be visualised in the parametric plane $[k_i, k_p]$ (Fig. 3). The boundary finding algorithm defining the set of admissible controllers was presented in [4].

$$\mathsf{K} \triangleq \{[k_p, k_i] : \|H(s,k)\|_\infty \leq \gamma\}$$

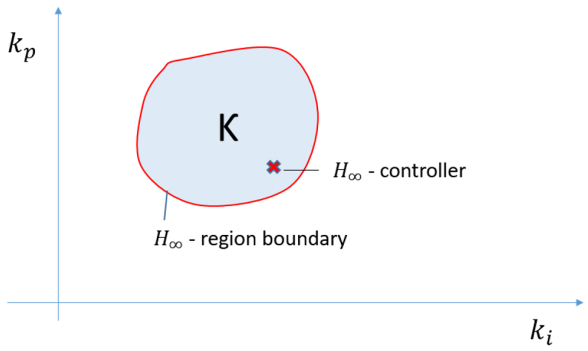

Fig. 3: H_∞ region and the admissible set $\mathcal{K}$ in the parametric $k_i - k_p$ plane of the PI controller

IV. Robust and optimal design for the collocated control setup

In case a nonempty set is found, one particular parameter combination has to be chosen. In [4]–[6], the point leading to the maximum integral gain was proposed that is known to minimise the integral error criterion

$$IE = \int_0^{+\infty} e(t)\mathrm{d}t = \frac{1}{k_i}. \tag{4}$$

However, this choice may not be viable for the formulated collocated control setup because of the following considerations:

- While the minimization of IE criterion proved to be useful for disturbance rejection in closed-loop systems with the aperiodic response (commonly encountered in the process control domain), it may not be a proper performance measure for oscillatory systems common in mechatronic applications.
- The user has no clue on how to reduce the controller gains systematically when only one point in the controller parametric space is given. This might be needed for practical implementation where performance vs robustness/energy consumption/noise amplification trade-offs appear.
- For the collocated control setup from Fig. 2, actuator side performance does not automatically guarantee good load-side behaviour. Multivariable and multi-objective control problem inherently arises.

To address the above-mentioned issues, we propose a modification of the previously described H_∞ regions method. The process of robust and optimal design of the fixed structure feedback controller C can be summarised in the following steps:

1) Define the model of the controlled plant, optionally including uncertainty for a robust control design
2) Define feedback and performance variables y and z for the collocated control setup, forming a single-input-two-outputs system (the simpler SISO scenario is also covered by choosing $y = z$)
3) Find a H_∞ region and the corresponding admissible set $\mathcal{K}$ in the parametric space of the controller fulfilling certain H-infinity loop shaping inequality to enforce robustness feedback loop formed via the output y
4) From the admissible set $\mathcal{K}$, find an optimal vector of controller parameters with respect to the defined performance variable z and a chosen performance measure
5) (optional) Provide a set of suboptimal reduced-gain controllers allowing in-situ fine-tuning of the controller during commissioning to find a suitable performance/cost trade-off

AD1 - Plant model definition: The model of the controlled plant can be, in principle, entered in several ways:

- Single deterministic linear-time-invariant (LTI) continuous or discrete-time model in the form of transfer function or state space representation
- Uncertain model set with a nominal plant plus unstructured uncertainty [10]
- Uncertain model set with a nominal plant plus a structured uncertainty, leading to a standard $N - \Delta$ model structure, with a block-diagonal matrix Δ defining the uncertain part [8]
- Uncertain model set defined by a finite count of assumed LTI plants (e.g. for a nonlinear controlled plant operating around several working points or along a trajectory)

AD3 - Robust controller set derivation: For this step, we formulate the following design constraint on the maximum sensitivity

$$M_s \triangleq ||S_y(s,k)||_\infty = \left|\left| \frac{1}{1 + C(s,k)P_y(s)} \right|\right|_\infty < \gamma, \quad (5)$$

where S_y is the sensitivity function corresponding to the feedback loop formed via the measured output y and γ is a user-specified hyper-parameter. The M_s criterion is a well-known measure of robustness in stability as it directly affects the disc stability margin $s_m = 1/M_s$, defined as the minimal distance of the open-loop frequency response function to the critical $[-1, j0]$ point in the complex plane, thus giving a geometric interpretation of allowed gain and phase uncertainty in the plant model.

In the case of uncertain plant models defined as a representative set of n LTI systems, the maximum sensitivity can be enforced for all the members as follows

$$\begin{aligned} &\max_{\forall i}\{M_{s,i}\} < \gamma, \\ &M_{s,i} = \left|\left| \frac{1}{1 + C(s,\boldsymbol{k})P_{y,i}(s)} \right|\right|_\infty, \ i = 1..n. \end{aligned} \quad (6)$$

In the case of models with unstructured uncertainty, other loop shaping inequalities arise. For example, when using a multiplicative uncertainty model

$$P_y(s) \triangleq P_n(s) + W_m(s)\Delta(s), \quad (7)$$

where P_n is a nominal model, Δ is a stable norm-bounded operator such that $||\Delta||_\infty \leq 1$ and W_m is a frequency-dependent scaling function, a robust stability condition can be derived in the form of

$$||W_m(s)T_n(s)||_\infty < 1, \quad (8)$$

with $T_n(s) = \frac{C(s)P_n(s)}{1+C(s)P_n(s)}$ denoting the nominal complementary sensitivity function. Similar results can be derived for other uncertainty model structures, see e.g. [10].

For the structured uncertainty model, the robustness in stability can be evaluated by means of the $M - \Delta$ test

$$\mu(M) < 1, \quad (9)$$

where M is the deterministic part of the system forming a feedback loop with the block-diagonal Δ operator and μ is the structured singular value [8]. For this particular case, the criterion (9) cannot be simply translated to the boundary in the controller parameter space as in the previous cases. However, it can be handled in the next step of controller optimization by evaluating the inequality (9) sample-wise in terms of a finite controller set.

AD4 - Performance optimisation: The region of robust admissible controllers $\mathcal{K}$ from step 3 is sampled by means of a grid with a chosen resolution, forming a finite set

$$\mathcal{K}_g\{i\} \triangleq \boldsymbol{k_i} = [k_{pi}, k_{ii}], \ i = 1..n_g : \ \mathcal{K}_g \subset \mathcal{K} \quad (10)$$

where $n_g = n(\mathcal{K}_g)$ is the cardinality of the set formed from the points on the grid inside the H_∞ region derived in step 3 and depends on the chosen sampling resolution.

The main reason for sampling/gridding is that the infinite number of robust controllers in the set $\mathcal{K}$ reduces to the set $\mathcal{K}_g$ with finite members, which allows simple further segmentation of suitable controllers based on secondary performance criteria that can be defined in time, algebraic or frequency domain, e.g.:

- Other classical robustness in stability measures – gain and phase margins
- Closed-loop bandwidth for the feedback or performance variable
- Damping of the closed-loop poles or their occurrence in a specified forbidden region of the complex plane
- Overshoot/settling times for any important closed-loop transfer function, either considering the feedback or performance variable as output
- Robustness in stability with respect to structured uncertainty evaluated by means of the structured singular value and criterion (9)
- Robustness in performance with respect to structured uncertainty evaluated by means of the structured singular value criterion $\mu(N) < 1$, where N is the deterministic part of the uncertain system in the standard $N - \Delta$ structure [8]

By performing this secondary segmentation, a new reduced set is formed

$$\mathcal{K}_s \subseteq \mathcal{K}_g,\ n_s = n(\mathcal{K}_s) \leq n_g \tag{11}$$

Subsequently, an optimal controller is found by minimizing (or maximizing) a chosen cost function. We found that well-known time-domain integral criteria provide good results in practical design problems, including e.g.

1) **ISE** (Integral of squared error)

$$J(\boldsymbol{k}) = \int_0^\infty [e(\tau, \boldsymbol{k})]^2 \mathrm{d}\tau \tag{12}$$

2) **IAE** (Integral of absolute error)

$$J(\boldsymbol{k}) = \int_0^\infty |e(\tau, \boldsymbol{k})| \mathrm{d}\tau \tag{13}$$

3) **ITAE** (Integral of time-weighted abs. error)

$$J(\boldsymbol{k}) = \int_0^\infty \tau |e(\tau, \boldsymbol{k})| \mathrm{d}\tau \tag{14}$$

4) **Quadratic cost function**

$$J(\boldsymbol{k}) = \int_0^\infty \alpha e(\tau, \boldsymbol{k})^2 + u(\tau, \boldsymbol{k})^2 \mathrm{d}\tau \tag{15}$$

The performance cost functions are evaluated for the load-concerned performance variable z, forming another finite set

$$\mathcal{J}_s\{i\} \triangleq J(\mathcal{K}_s\{i\});\ n(\mathcal{J}_s) = n_s, \tag{16}$$

with the entries coupled to the controller set $\mathcal{K}_s$. The error signal $e(t, \mathbf{k})$ that depends on the controller gains can be evaluated either from the reference step response to emphasize tracking performance in servo problems or for disturbance step response to accentuate the closed-loop disturbance rejection capability. Any meaningful combination/function of multiple cost functions can also be evaluated.

The optimal controller is found by minimizing a chosen performance cost function as

$$C^*(s, \boldsymbol{k}^*) : \boldsymbol{k}^* = \mathcal{K}_s\{\underset{\forall i}{argmin}\ \mathcal{J}_s\{i\}\} \tag{17}$$

The minimum value can simply be found due to the finite cardinality of the sets $\mathcal{K}_s, \mathcal{J}_s$. In practice, the true global minimum with respect to cost functions (12)-(15) and the infinite set $\mathcal{K}$ may lie outside of the sampled data points of the chosen grid. This true global optimum may optionally be approached by means of standard numerical optimisation algorithms, with the result (17) chosen as the initial condition. However, the difference may be negligible for sufficiently dense resolution of the grid.

Working with the finite sets of sampled and segmented controllers offers some key advantages compared to attempts of direct parametric optimisation:

1) Utilisation of numerical optimisation methods that are sensitive to initial conditions and can converge to local minima is avoided, considerably increasing the chance of finding the truly global optimal solution
2) Multi-objective optimisation is possible by combining time-, algebraic- and frequency-domain design requirements
3) The performance measure can be evaluated for uncertain plants defined as model sets by forming (weighted) average or worst-case performance measures from the cost functions evaluated for the individual plant models
4) Systematic selection of suboptimal controllers with reduced closed-loop bandwidth is possible, providing complementary information useful for practical controller implementation and tuning

AD5 - Suboptimal controller set derivation: There might be cases where the optimal controller from step 4 does not work well when employed on the real plant. This is typically due to controller gains that are too high, causing problems with either stability, noise amplification or insufficient robustness with respect to unmodelled dynamics. Gain reduction to achieve a more conservative tuning often helps to alleviate these problems. However, to avoid the necessity of iterative hand-tuning the controller again in this phase of commissioning, a systematic guide is provided in our method.

The admissible controller space is divided into a specified number of m subsets $\mathcal{S}_l$ on the sampled grid based on the values of the chosen performance cost from the previous step

$$\mathcal{S}_l \triangleq \{\forall \boldsymbol{k} \in \mathcal{K}_s :\ J^l_{min} \leq \mathcal{J}_s \leq J^l_{max}\}, \bigcup_{\forall l} \mathcal{S}_l = \mathcal{K}_s,\ l = 1..m \tag{18}$$

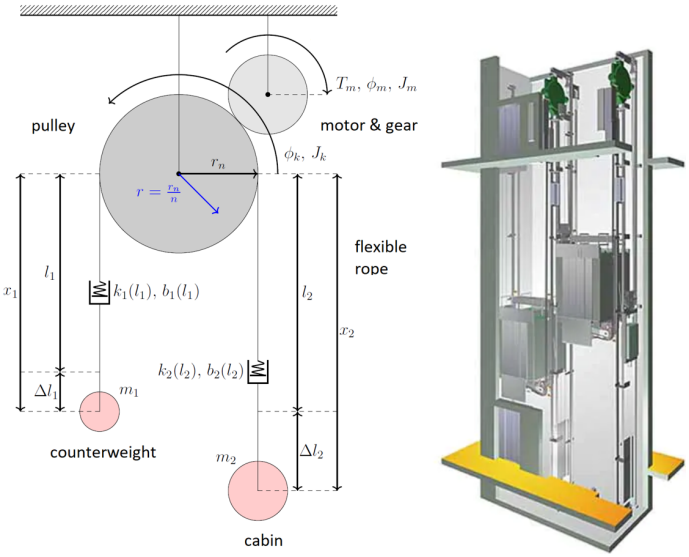

Fig. 4: Lift control problem - positioning of the cabin by means of an electrical drive

Consequently, m suboptimal controllers are derived from the same number of S_k sets by minimizing the same (or some other) secondary cost function J_m

$$\boldsymbol{k}_{sub}^{l} = \mathcal{K}_s\{\underset{\forall i \in \mathcal{S}_l}{argmin}\ \mathcal{J}_m\{i\}\},\ l = 1..m, \tag{19}$$

where $\mathcal{J}_m\{i\}$ is defined in the same way as for the primary cost J in (16).

In this way, the controller gains and closed-loop bandwidth can be systematically reduced while preserving the optimality of the achieved solution in terms of the cost functions J, J_m and robustness in stability since the search in the parametric space is constrained to stay in the admissible robust controller set $\mathcal{K}$.

V. Lift control benchmark problem

For the experimental validation of the proposed method, the lift control system defined as one of the Use case applications of the IMOCO4E project was chosen as a representative benchmark problem. We consider a lift system depicted in Fig. (4). A first-principle model can be derived in the form of a flexible multi-body model consisting of the passenger cabin, counterweight, driving pulley and motor with gear. Oscillatory behaviour is observed due to the inherent flexibility of the rope. Any unwanted transient and residual oscillations can be dangerous for the machinery and reduce passenger comfort [11]. They should be mitigated at by proper parameterisation of the drive motion control system [12].

TABLE I: Parameters of the lift system model

Parameter	*Value*
gear ratio n	15
gravity constant g	9.81 $\frac{m}{s^2}$
counterweight mass m_1	1000 kg
cabin mass m_2	600 - 1400 kg
pulley mass m_k	50 kg
total rope length l_0	33m
rope stiffness coefficient k_0	5e6 $\frac{N}{m}$
rope damping coefficient b_0	6e4 $\frac{N.s}{m}$
pulley radius r_n	0.3 m
motor inertia J_m	1e-4 $kg.m^2$
pulley inertia J_k	2.25 $kg.m^2$

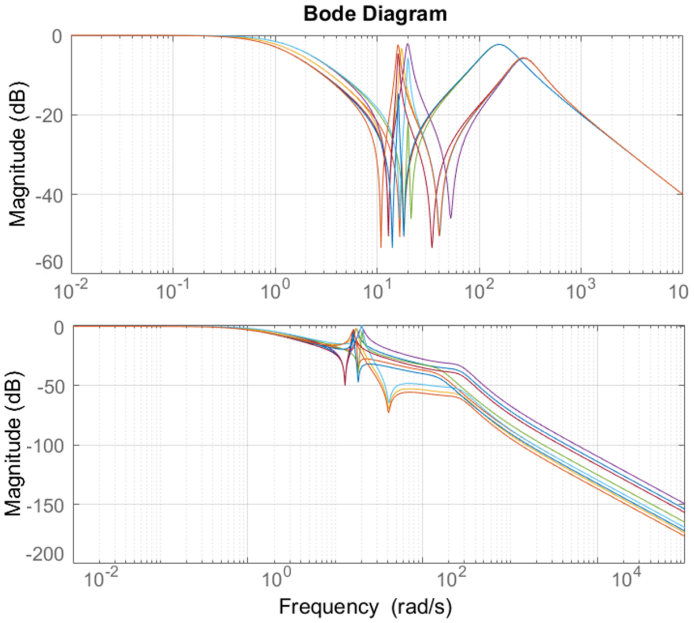

Fig. 5: Frequency response functions from motor torque to motor velocity (top) and cabin velocity (bottom) for nine different combinations of floor position and cabin mass

The multi-body system dynamics is governed by the following equations of motion

$$\begin{aligned}
\ddot{x}_1 &= g - \frac{k_0}{m_1(\phi r - \pi r)}(x_1 - \phi r + \pi r) - \frac{b_0}{m_1(\phi r - \pi r)}(\dot{x}_1 - \dot{\phi} r) - \frac{F_{f1}}{m_1} \\
\ddot{x}_2 &= g - \frac{k_0}{m_2(l_0 - \phi r)}(x_2 - l_0 + \phi r) - \frac{b_0}{m_2(l_0 - \phi r)}(\dot{x}_2 + \dot{\phi} r) - \frac{F_{f2}}{m_2} \\
\ddot{\phi} &= \frac{T}{J} + \frac{k_0 r}{J(\phi r - \pi r)}(x_1 - \phi r + \pi r) + \frac{b_0 r}{J(\phi r - \pi r)}(\dot{x}_1 - \dot{\phi} r) + \dots \\
&\dots - \frac{k_0 r}{J(l_0 - \phi r)}(x_2 - l_0 + \phi r) - \frac{b_0 r}{J(l_0 - \phi r)}(\dot{x}_2 + \dot{\phi} r) - b_f \frac{\dot{\phi}}{J}, \\
J &= J_m + \frac{J_k}{n^2}, r = \frac{r_n}{n}
\end{aligned} \tag{20}$$

where x_1, x_2, ϕ stand for counterweight, cabin and motor pulley position, T is the actuator torque, $F_{f1,2}$ denote friction forces, and other physical parameters given in table I.

A specific challenge of the lift system comes from its position-dependent oscillatory dynamics due to the variable active length of the rope segments. This is demonstrated for a specific set of physical parameters given in table I by

observing the frequency response functions computed from the linearized models, where the cabin mass and position were varied (Fig. 5). Two dominant resonance/antiresonance pairs are observed due to the flexibility of the ropes with the hanging load. Their location varies as a function of cabin mass and position.

The oscillatory behaviour must be attenuated to ensure safe and reliable operation. This can be done by the proper design of the feedback controller. For this moment, we assume that a fixed parameter PI velocity controller commonly used in industrial drive systems in the form of

$$C(s) = \frac{T(s)}{e(s)} = k_p + \frac{k_i}{s}, \tag{21}$$

where k_p, k_i denote proportional and integral gains, T denotes the output torque generated by the drive, and e denotes the actual velocity error. The controller parameters must be tuned to achieve satisfactory cabin-side performance, while the loop is typically closed via the motor-side feedback since most lift installations do not allow simple direct measurement of cabin position and/or velocity. Therefore, the control topology matches the collocated control setup formulated in the previous section (Fig. 2).

STEP 1 - Plant model definition: The uncertain model set is constructed from 9 samples of representative LTI models acquired from different combinations of cabin positions (three different floors in a building, $l_2 = \{3, 15, 30\}m$) and three distinct cabin loads ($m_2 = \{600, 1000, 1400\}kg$). The robust controller should work well for all the assumed cases of parametric variations that influence the plant dynamics in different operating points.

STEP 2 - Collocated control setup: Motor-side velocity is defined as the feedback variable y, while the cabin velocity becomes the performance output z, forming a single-input-two-outputs system from Fig. 2.

STEP 3 - Robust controller design: The loop shaping inequality defining the robust control set $\mathcal{K}$ is formulated in the form of maximum sensitivity

$$\mathcal{K} \triangleq \{\boldsymbol{k} : \max_{\forall i}(M_{s,i}) \leq 1.8\}, \tag{22}$$
$$M_{s,i} = \left|\left| \frac{1}{1 + C(s)P_{y,i}(s)} \right|\right|_\infty, \; i = 1..9$$

which has to be fulfilled for the whole uncertain model set containing nine representative transfer functions for different working points and variable load. Fig. 6 shows the resulting H_∞ region $\mathcal{K}$ designating the set of admissible controllers fulfilling the robustness requirement (22).

Step 4 - Performance optimisation: From the admissible set $\mathcal{K}$, one particular controller has to be chosen for implementation. While all the controllers provide the desired robustness in stability, they differ considerably in the achieved closed-loop performance. One could possibly opt for the solution with the highest integral gain, according to the IE criterion (4) proposed

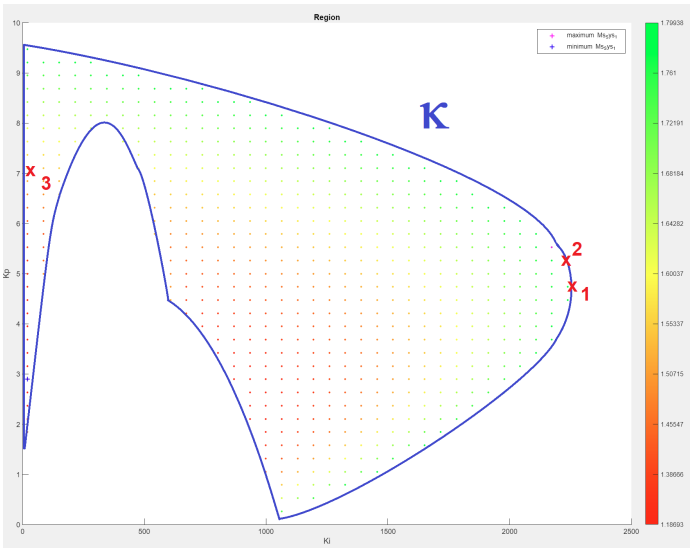

Fig. 6: Admissible region $\mathcal{K}$, the dots represent the finite set $\mathcal{K}_g$ (22) with colour corresponding to the maximum achieved M_{si} value, red x-marks denote optimal controllers; 1 - IE criterion, 2 - ITAE criterion for y variable, 3 - ITAE criterion for z variable

in the earlier studies [4], [5], as designated by x-mark Nr. 1 in Fig. 6. This leads to the control gain vector

$$\boldsymbol{k}_1 = [k_p, k_i] = [4.47, 2330]. \tag{23}$$

Fig. 7 shows the resulting closed-loop reference step responses for the set of representative nine plant models. While a decent performance is observed at the motor side for the feedback variable y, severe cabin-side vibrations arise. This is a typical scenario for collocated motion setups, where a high-gain controller closing the feedback loop at the actuator side excites an unacceptable level of load-side oscillations. Changing the performance criterion does not help in this case. Switching from IE cost (4) to the total/average ITAE (14) cost

$$J_t^y(\boldsymbol{k}) \triangleq \sum_{\forall i} \int_0^\infty \tau |e_i^y(\tau, \boldsymbol{k})| \mathrm{d}\tau, \tag{24}$$
$$e_i^y(\tau, \boldsymbol{k}) = w_1 - y_i = \mathcal{L}^{-1}\left\{ \frac{1}{s} \frac{1}{1 + C(s, \boldsymbol{k})P_{y,i}(s)} \right\}, \tag{25}$$

leads to a controller $\boldsymbol{k}_2 = [5.2, 2260]$ (Fig. 6) with a closed-loop behaviour very close to that of the IE solution from Fig. 7. A load-concerned tuning is necessary, taking the second output z as the input for the performance optimisation.

When choosing the cabin-side output z as the performance variable and recomputing the optimization problem for the new cost function defined using the cabin-side error as follows

$$J_t^z(\boldsymbol{k}) \triangleq \sum_{\forall i} \int_0^\infty \tau |e_i^z(\tau, \boldsymbol{k})| \mathrm{d}\tau, \tag{26}$$
$$e_i^z(\tau, \boldsymbol{k}) = w_1 - z_i = \mathcal{L}^{-1}\left\{ \frac{1}{s} \frac{1 + C(P_{y,i} - P_{z,i})}{1 + C(s, \boldsymbol{k})P_{y,i}(s)} \right\}. \tag{27}$$

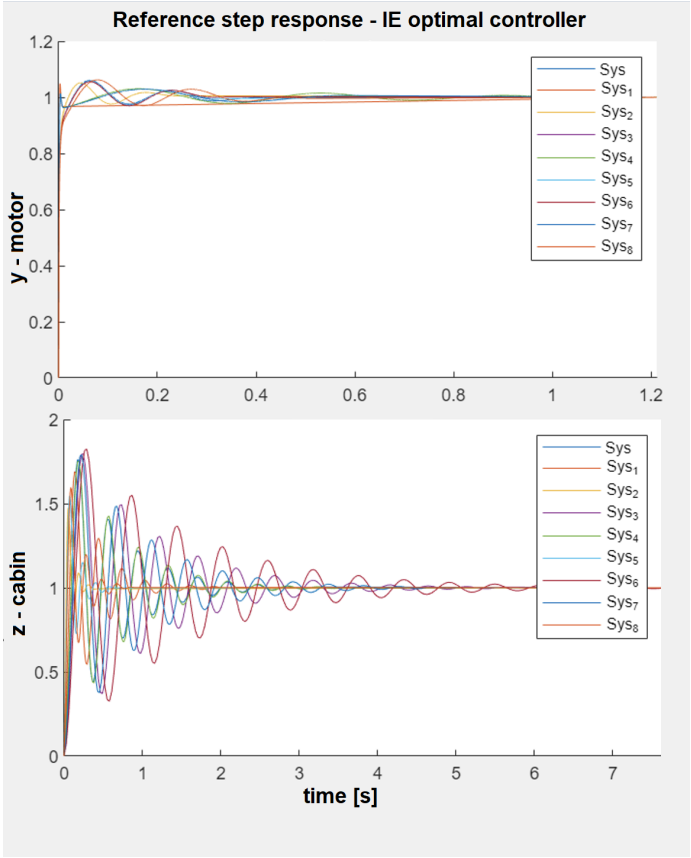

Fig. 7: Closed-loop performance achieved with IE optimal controller k_1 - motor and cabin-side reference step response

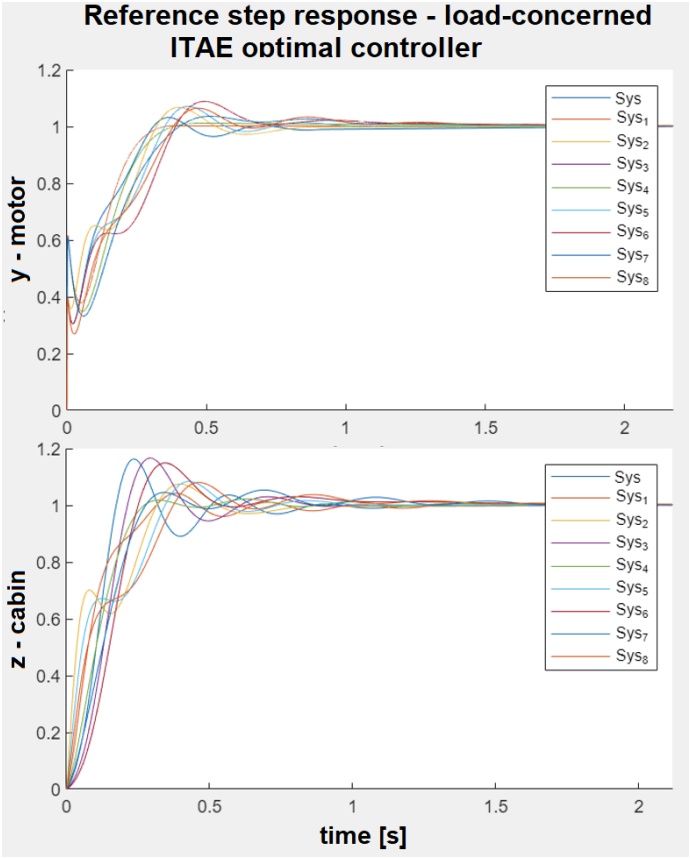

Fig. 8: Closed-loop performance achieved with load-concerned ITAE optimal controller k_3 - motor and cabin-side reference step response

The optimal controller is obtained with the gain vector

$$\boldsymbol{k}_3 = [k_p, k_i] = [7.1, 9.7]. \tag{28}$$

Fig. 8 displays the resulting closed-loop performance in terms of motor and cabin velocity response to step reference change. The settling time at the motor side is longer than for the IE controller. However, cabin-side performance is improved considerably, showing much better damped transients with less overshoot.

Apart from linear analysis using the uncertain model set, also a full-scale nonlinear simulation was performed, linking the optimal controller (28) and model (20). Jerk-limited piecewise polynomial reference trajectory profile shown in Fig. 9 was generated using the algorithms derived in [13], [14]. It simulates the scenario of a rest-to-rest manoeuvre used for positioning the lift cabin between two different floors. Fig. 10 shows the resulting tracking performance. Smooth velocity and acceleration response is achieved without exhibiting any cabin-side vibrations. This validates the proper design of the robust and optimal controller.

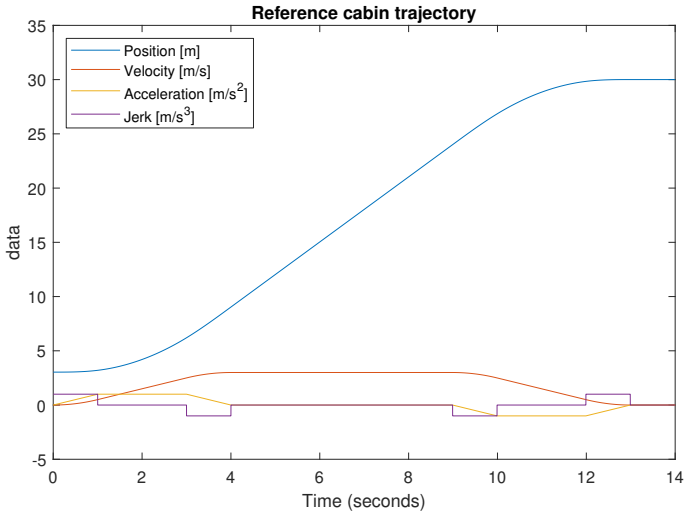

Fig. 9: Reference lift point-to-point motion trajectory

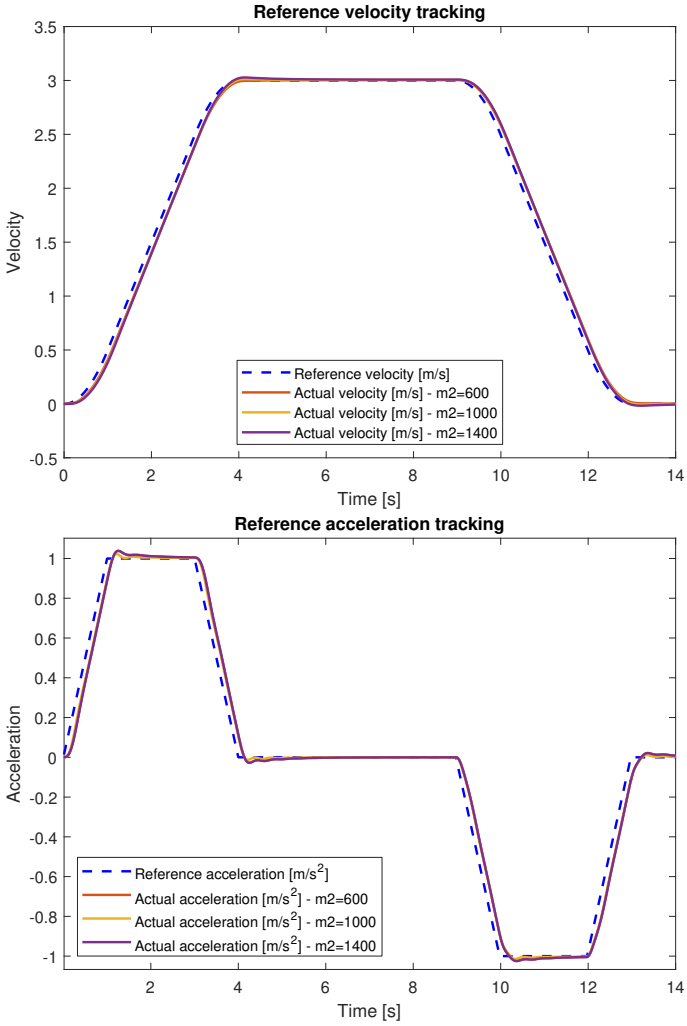

Fig. 10: Velocity (top) and acceleration (bottom) tracking performance during ten floors traversal for three distinct cabin load values $m_2 = \{600, 1000, 1400\}kg$

VI. Summary

The paper describes a methodology suitable for the derivation of robust and optimal low-order fixed structure controllers. An emphasis is given to the collocated control setup, which is commonly used in mechatronic systems with oscillatory dynamics and motor-mounted sensor used for closing the feedback loop. Care must be taken in such cases to achieve satisfactory load-side performance. The advantage of the presented method is the ability to combine the robustness and optimality aspects while deriving simple controllers that are easily implementable in practice. The method can be modified to other PID-type compensators with two or three parameters. Multi-objective performance optimisation is possible, combining various time- algebraic- or frequency-domain criteria, which is achieved by means of sampling and segmenting the robust admissible controller set. The lift control problem is studied as a benchmark use case, demonstrating the practical applicability of the proposed approach.

VII. Future work

Our future work will be directed to the development of a user-friendly supporting software tool suitable for designing low-order robust and optimal controllers in terms of the formulated collocated control setup. Also, a design of feedforward controllers supplementing the feedback loop to further improve performance of a motion system will be a next research direction.

Acknowledgment

This research was performed within the 'Intelligent Motion Control under Industry4.E' (IMOCO4.E) project [15], which has received funding from the ECSEL Joint Undertaking under grant agreement No. 101007311.

References

[1] M. Steinbuch, T. Oomen, and H. Vermeulen, "Motion control, mechatronics design, and Moore's law," *IEEJ Journal of Industry Applications*, vol. 11, no. 2, pp. 245–255, 2022.

[2] T. Oomen, "Advanced motion control for precision mechatronics: Control, identification, and learning of complex systems," *IEEJ Journal of Industry Applications*, vol. 7, no. 2, pp. 127–140, 2018.

[3] K. J. Åström and T. Hägglund, "Revisiting the ziegler–nichols step response method for pid control," *Journal of process control*, vol. 14, no. 6, pp. 635–650, 2004.

[4] M. Schlegel and P. Medvecová, "Design of PI controllers: H-infinity region approach," *IFAC-papersonline*, vol. 51, no. 6, pp. 13–17, 2018.

[5] M. Goubej and M. Schlegel, "PI plus repetitive control design: H-infinity regions approach," in *2019 22nd International Conference on Process Control (PC19)*. IEEE, 2019, pp. 62–67.

[6] M. Goubej, J. Königsmarková, R. Kampinga, J. Nieuwenkamp, and S. Paquay, "Employing finite element analysis and robust control concepts in mechatronic system design-flexible manipulator case study," *Applied Sciences*, vol. 11, no. 8, 2021. [Online]. Available: https://www.mdpi.com/2076-3417/11/8/3689

[7] V. Žán, K. Kubíček, and M. Čech, "Design of robust PI controller by combining robustness regions with time-domain criteria," in *2022 IEEE 27th International Conference on Emerging Technologies and Factory Automation (ETFA)*. IEEE, 2022, pp. 1–8.

[8] S. Skogestad and I. Postlethwaite, *Multivariable feedback control: analysis and design*. john Wiley & sons, 2012.

[9] J. Doyle, K. Glover, P. Khargonekar, and B. Francis, "State-space solutions to standard h2 and h-infinity control problems," in *1988 American Control Conference*. IEEE, 1988, pp. 1691–1696.

[10] J. C. Doyle, B. A. Francis, and A. R. Tannenbaum, *Feedback control theory*. Courier Corporation, 2013.

[11] B. Z. Knezevic, B. Blanusa, and D. P. Marcetic, "A synergistic method for vibration suppression of an elevator mechatronic system," *Journal of Sound and Vibration*, vol. 406, pp. 29–50, 2017.

[12] C. Li, J. Lu, J. Lai, J. Yao, and G. Xiao, "Assessment of ride comfort of traction elevators using iso 18738-1: 2012 and iso 2631-4: 2001 standards," *Journal of Intelligent Manufacturing and Special Equipment*, no. ahead-of-print, 2022.

[13] M. Blejan and R. Blejan, "Mathematics for real-time s-curve profile generator," *Hidraulica*, no. 4, pp. 7–25, 2020.

[14] L. Bláha, M. Schlegel, and J. Mošna, "Optimal control of chain of integrators with constraints," in *2009 17nd International Conference on Process Control (PC09)*. IEEE, 2009, pp. 51–56.

[15] M. Čech, A.-J. Beltman, and K. Ozols, "Digital Twins and AI in Smart Motion Control Applications," in *2022 IEEE 27th International Conference on Emerging Technologies and Factory Automation (ETFA)*. IEEE, 2022, pp. 1–7.